



UNIVERSITY OF LEEDS

This is a repository copy of *Quantifying Passive Ventilation within Small Livestock Trailers using Computational Fluid Dynamics*.

White Rose Research Online URL for this paper:  
<http://eprints.whiterose.ac.uk/97368/>

Version: Accepted Version

---

**Article:**

Gilkeson, CA, Thompson, HM, Wilson, MCT et al. (1 more author) (2016) Quantifying Passive Ventilation within Small Livestock Trailers using Computational Fluid Dynamics. *Computers and Electronics in Agriculture*, 124. pp. 84-99. ISSN 0168-1699

<https://doi.org/10.1016/j.compag.2016.03.028>

---

© 2016, Elsevier. Licensed under the Creative Commons Attribution-NonCommercial-NoDerivatives 4.0 International  
<http://creativecommons.org/licenses/by-nc-nd/4.0/>

**Reuse**

Unless indicated otherwise, fulltext items are protected by copyright with all rights reserved. The copyright exception in section 29 of the Copyright, Designs and Patents Act 1988 allows the making of a single copy solely for the purpose of non-commercial research or private study within the limits of fair dealing. The publisher or other rights-holder may allow further reproduction and re-use of this version - refer to the White Rose Research Online record for this item. Where records identify the publisher as the copyright holder, users can verify any specific terms of use on the publisher's website.

**Takedown**

If you consider content in White Rose Research Online to be in breach of UK law, please notify us by emailing [eprints@whiterose.ac.uk](mailto:eprints@whiterose.ac.uk) including the URL of the record and the reason for the withdrawal request.



[eprints@whiterose.ac.uk](mailto:eprints@whiterose.ac.uk)  
<https://eprints.whiterose.ac.uk/>

# Quantifying Passive Ventilation within Small Livestock Trailers using Computational Fluid Dynamics

C.A. Gilkeson<sup>a1</sup>, H.M. Thompson<sup>a2</sup>, M.C.T. Wilson<sup>a3</sup> and P.H. Gaskell<sup>b4</sup>

<sup>a</sup>School of Mechanical Engineering, University of Leeds, Leeds, LS2 9JT, United Kingdom.

<sup>b</sup>School of Engineering and Computing Sciences, Durham University, South Road, Durham, DH1 3LE, United Kingdom.

<sup>1</sup>corresponding author: C.A.Gilkeson@leeds.ac.uk

<sup>2</sup>H.M.thompson@leeds.ac.uk

<sup>3</sup>M.Wilson@leeds.ac.uk

<sup>4</sup>P.H.Gaskell@durham.ac.uk

## Abstract

This paper illustrates three different methods which can be used to quantify passive ventilation inside small livestock trailers. Accomplishing this is crucial to determine whether animal welfare ventilation standards are met during road transport. High-fidelity Computational Fluid Dynamics (CFD) simulations are conducted for a detailed livestock trailer containing 48 sheep and coupled to a generic towing vehicle. An initial correlation study shows that the observed airflow patterns share the general flow structure with an equivalent but simplified geometry which has previously been validated. Further analysis of the detailed geometry shows that twice as much air flows through the upper deck of the trailer compared to the lower deck which is due to a tailboard vent allowing easier passage to the low-pressure wake. Ventilation is analysed using the net flow rate through vent openings along the side of the trailer; it is found to be below the regulatory threshold for vehicle speeds of up to 17.9 m/s on the lower deck and 8.9 m/s on the upper one. One drawback of this analysis method is that it does not consider ventilation efficacy within the interior. In order to address this, two additional methods are proposed to identify ventilation rates using (i) passive scalars and (ii) a particle tracking algorithm. The former method suggests that the greatest residence time is 30.0 s with the latter

indicating a value of 19.5 s; both of these occur in the vicinity of one animal muzzle, in a stagnant airflow region of the lower deck. All three analysis methods are compared to EU-specified regulatory ventilation rates in the form of a ventilation coefficient. Overall, ventilation is shown to be significantly better on the upper deck of the trailer, satisfying current livestock transport regulations at moderate to high vehicle speeds, whereas ventilation is markedly less on the lower deck and potentially below the regulatory threshold.

## Keywords

CFD; Livestock Trailer; Vehicle Aerodynamics; Ventilation.

## Highlights

- Three contrasting numerical methods successfully characterise passive ventilation
- Ventilation is better on the upper deck due to rear tailboard vent
- Ventilation coefficient highlights potential issues on the lower deck
- Welfare legislation for livestock transport discussed as well as proposed design modifications

## 1. Introduction

Safely moving livestock between farms, markets and abattoirs is an essential part of modern farming. Sheep, cattle, pigs and chickens are typically carried in one of two general types of vehicle, either small livestock trailers or large transporters. Both classes of vehicle comprise a lightweight chassis-mounted metal box structure which consists of open rectangular apertures spanning the vehicle sides. Passive ventilation is delivered through these apertures via air exchange between the internal environment and the external free airstream by virtue of vehicle movement (Hoxey *et al.*, 1996, Mitchell and Kettlewell, 2008). This serves to remove heat, moisture and other species such as CO<sub>2</sub> to control animal comfort levels (Randall and Patel, 1994). Active ventilation strategies involving fans have also shown merit in maintaining even internal airflow and temperature distributions within large vehicles (Kettlewell *et al.*, 2000, 2001). However, in more restricted scenarios such as livestock transporters contained on board ferries, natural ventilation can outperform mechanical ventilation (Norton *et al.*, 2013).

Broadly speaking the majority of previous studies have focussed on larger transporters. These include a noteworthy investigation of dual-unit poultry transporters carried out by the Silsoe Research Institute in 1996 (Hoxey *et al.*, 1996; Baker *et al.*, 1996 & Dalley *et al.*, 1996). Hoxey *et al.* (1996) conducted full-scale

experiments with the purpose of measuring surface pressure distributions during transit so that important features including locations of flow separation and reattachment, could be deduced. A combination of flow visualisation techniques and pressure measurements showed that the bluff shape of the transporter induced low-pressure flow separation around the front section of the upstream unit, followed by flow reattachment further downstream. The pressure distribution induced an internal flow direction which was predominantly back-to-front in the upstream unit (i.e. opposing the external free-stream direction); however, the lack of a pressure gradient in the second (downstream) unit meant that no dominant flow structure was seen. Pressure variations due to local turbulent fluctuations were small due to the reduced time scales and so they had a minimal impact on ventilation. In contrast the mean pressure distribution was found to be the determining factor in sustaining bulk air movement through the vehicle (Hoxey *et al.*, 1996).

In an attempt to directly quantify ventilation, Purswell *et al.* (2005) investigated the air exchange rates in a large horse trailer during transit. The trailer was 9.1 m long with an empty volume of 41.5 m<sup>3</sup>. Decay rates of a tracer gas, namely carbon dioxide, were measured in various locations to give estimates of the net air exchange rate. Ventilation was limited at the front of the trailer which is shielded from the free-stream by the headboard. This observation is consistent with the high temperatures seen in the same region of other transporters, due to reduced air movement (Dalley *et al.*, 1996; Quinn and Baker, 1997). Furthermore, the air exchange rate averaged over a range of vehicle speeds and ventilation configurations fell from 0.60 air changes/minute (ACM) for the empty trailer to 0.49 ACM with horses on board, implying that the presence of animals reduces ventilation, probably due to increased blockage. Notable variations in the exchange rate throughout the trailer were reported, highlighting the difficulty of measuring ventilation rates in practice, as they are highly turbulent. The most significant conclusion was that the horse transporter is under-ventilated compared to recommendations for stabled horses (Wheeler, 2003); this observation was true for any combination of vehicle speed or configuration tested.

More recent studies relating specifically to small livestock trailers illustrate the difference in ventilation rates between upper and lower decks; air movement on the lower deck is generally much less than the upper one (Gilkeson *et al.*, 2006, 2009; Gilkeson 2009). These observations are based on 1/7<sup>th</sup> scale wind tunnel experiments and corresponding Computational Fluid Dynamics (CFD) results. The purpose of this investigation is to extend these studies to full-scale livestock trailers, incorporating animals, to assess the impact of vehicle speed on the passive ventilation characteristics. This is achieved using CFD to simulate the complex flow field within the trailer before considering a range of analyses to better understand the ventilation characteristics within this region.

## 2. Methodology

Characterising passive ventilation within small livestock trailers is challenging due to the coupled nature of the internal air volume and the external flow field. Whilst a decoupled approach may be suitable in cases where the internal flow can be analysed in isolation (e.g. within refrigerated vehicles), the supply of ventilation to livestock trailers relies on open vent apertures. Air exchange through these is driven by the pressure field around the vehicle during transit (Hoxey *et al.*, 1996; Gilkeson *et al.*, 2009). It follows that a computational solution domain should consist of the coupled internal and external air volumes, to capture the ventilation exchange between these distinct regions. This section describes the numerical approaches used to achieve this.

### 2.1 Geometry

Figure 1(a) shows a CAD model of the generic livestock trailer and towing vehicle used. The trailer consists of two decks, each with a series of six rectangular vent openings on both the left and right side panels. The upper deck has a supplementary larger vent opening above the tailboard of the trailer as shown in Figure 1(b). The tailboard also serves as a ramp to load livestock onto the trailer which prevents further rear-facing vent apertures from being used; this is a significant design constraint as will be discussed later. For comparison, the actual trailer used as the basis for the CAD model is presented in Figure 1(c). External features including the outer ribs, wheels and wheel arch structures are included in the geometry; however, finer details such as gaps between panels are omitted for simplicity.

Internally, it is necessary to represent the animal mass to accurately represent the reduced air volume within the trailer; this is known to influence the internal flow patterns within passively ventilated transport vehicles (Purswell *et al.*, 2005; Gilkeson *et al.*, 2009). As this particular type of livestock trailer is commonly used to transport sheep, the internal geometry should resemble the characteristics of this species of animal. Figures 2(a) and (b) present two early developments of the animal mass with varying levels of detail. The final design, shown in Figure 2(c), embodies the high animal packing density typically used in practice with a series of protruding sheep head structures above the primary mass. This idea is similar to the implementation of cattle shapes in a recent CFD investigation of ventilation during ferry transport (Norton *et al.*, 2013). In the present study, the number of sheep per deck, 24, is calculated based on the maximum permissible animal load of 35 kN for a trailer of this size. The orientation of each head shape is varied randomly at angles in the range  $\pm 30$  degrees to the longitudinal axis, together with a staggered spatial distribution, when viewed from above. The main container unit measures 3.66 m long, 1.82 m wide and 1.81 m high, leading to internal air volumes of 0.64 m<sup>3</sup> and 1.01 m<sup>3</sup> on the lower and upper decks, respectively.

Note that these volumes account for the displacement of air due to the animal masses; the air volume contained within the empty trailer is significantly greater.

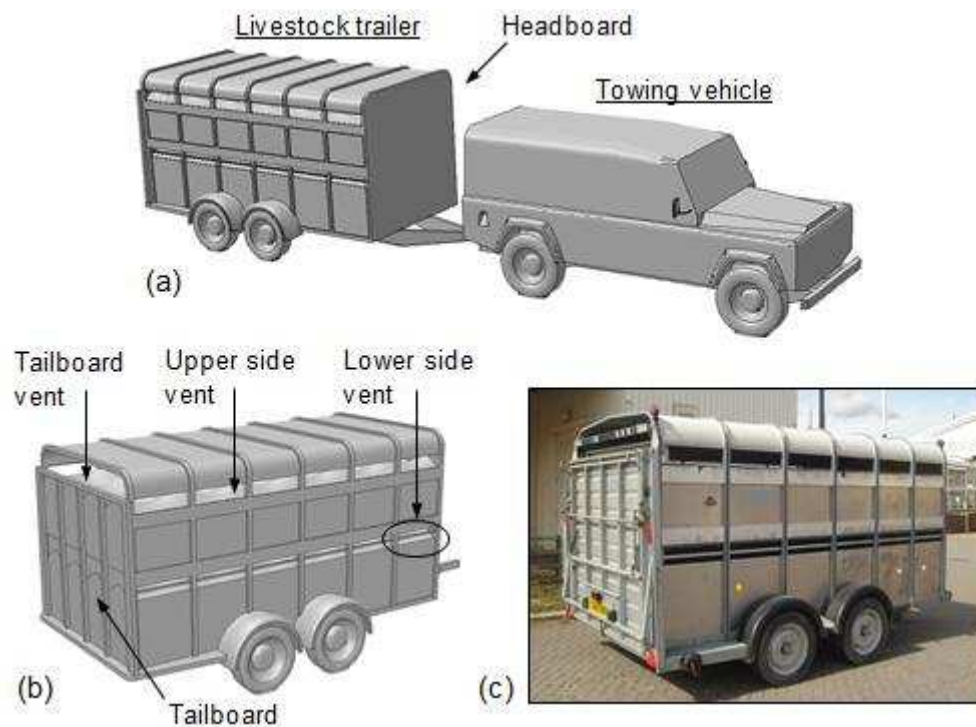


Figure 1: CAD model showing (a) the generic towing vehicle and livestock trailer, (b) rear view of the trailer only and (c) photograph of the trailer design forming the basis of the model.

The external shape of the solution domain is defined in terms of the combined length of the vehicles,  $L = 9.522$  m. The domain cross section is based on one-quarter of an ellipse with a ground level radius of  $5L$  and a ground-to-ceiling radius of  $4L$ ; this shape effectively fits around both vehicles whilst saving overall volume compared to a rectangular domain. A symmetry plane is employed to reduce the computational effort. The upstream boundary, a velocity inlet, is placed  $5L$  ahead of the towing vehicle and a pressure outlet is located  $20L$  downstream of the trailer, giving a total domain length of  $26L = 247.5$  m, see Figure 3. Results from preliminary simulations verified the suitability of these dimensions which are sufficiently large to allow the ambient air to flow naturally towards the vehicles and for the wake to be adequately captured downstream. Results showed that the intensity of the turbulent wake reduced along the length of the domain such that the pressure at the outlet was within 1 Pa of the required atmospheric value. Based on the frontal area of the vehicles, the blockage was very small at 0.2% and so this domain can be considered representative of a livestock trailer being towed in an unrestricted, free-airstream.

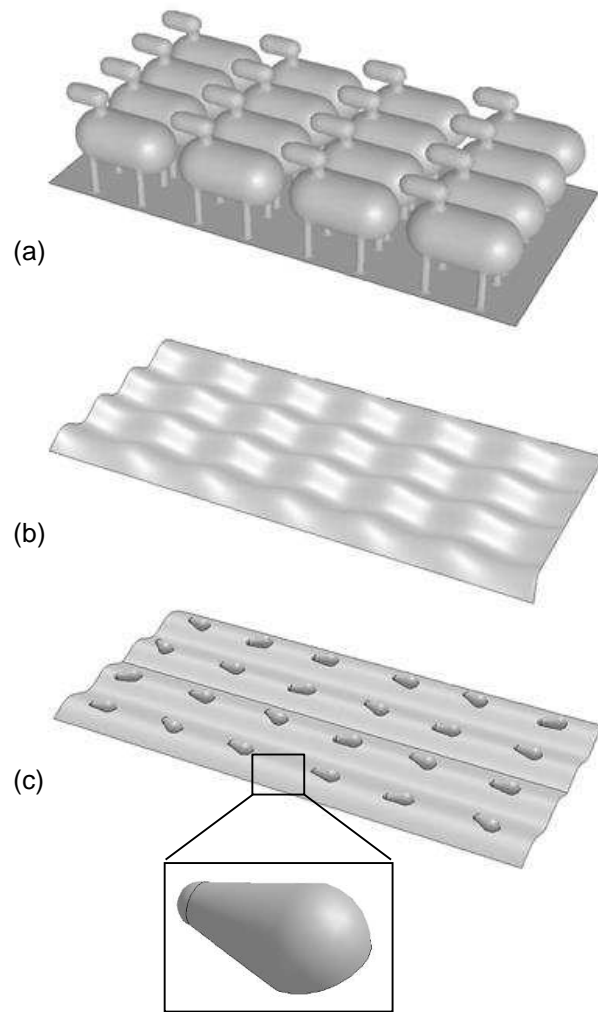


Figure 2: Various geometrical representations of one deck of sheep including (a) highly-detailed model, (b) upper surface of a simplified model and (c) the final design including protruding head structures.

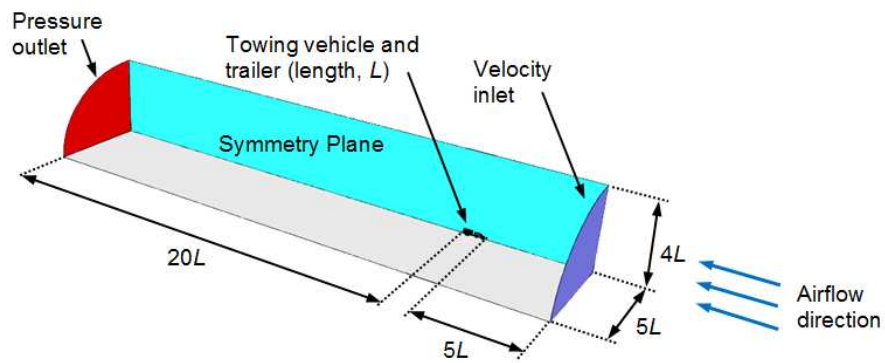


Figure 3: View of the solution domain.

## 2.2 Boundary Conditions

Table 1 summarises the boundary conditions required to simulate the aerodynamic flows at a slow vehicle speed of 4.47 m/s (10 mph). As with wind tunnel testing, it is customary to keep the vehicles stationary and to move the air and the ground relative to these which is equivalent to the vehicles moving through still air. Accordingly, the boundary conditions account for the angular velocity,  $\omega$ , of the wheels on both vehicles and the translational velocity,  $U$ , of the moving ground plane. All remaining walls are stationary with the no slip condition applied. The turbulence intensity,  $I$ , is assumed to be small in the free-stream with a value of 0.25% prescribed at both the velocity inlet and the pressure outlet. This represents a low turbulence intensity and is consistent with still ambient weather conditions; investigating the sensitivity of  $I$  on the ventilation rates for various wind characteristics is beyond the scope of this study. An equally important parameter is the turbulent length scale,  $L_T$ , defined as 7% of the characteristic length (ANSYS Fluent, 2013) which is taken as the combined length of both vehicles. The resulting turbulent length scale of 0.67 m is applied to both the inlet and outlet boundaries so that appropriate background turbulence levels are prescribed. For the simulations described later, five free-stream velocities representing vehicle speeds of 4.47 m/s, 8.94 m/s, 13.41 m/s, 17.88 m/s and 22.35 m/s were used, corresponding to 10 mph, 20 mph, 30 mph, 40 mph and 50 mph, respectively. The boundary conditions, see Table 1, are adjusted for each speed accordingly.

Table 1: Boundary conditions for a slow vehicle speed of 4.47 m/s.

Boundary Name	Boundary Type	Details
Vehicle surfaces	Stationary wall	No Slip
Trailer wheels	Rotating wall	No Slip, $\omega = 13.75$ rad/s
Towing vehicle wheels	Rotating wall	No Slip, $\omega = 11.46$ rad/s
Ground plane	Moving wall	No Slip, $U = 4.47$ m/s
Ceiling	Stationary wall	Zero shear stress
Inlet	Velocity inlet	$U = 4.47$ m/s, $I = 0.25\%$ , $L_T = 0.67$ m
Outlet	Pressure outlet	$p = 0$ Pa, $I = 0.25\%$ , $L_T = 0.67$ m
Symmetry plane	Symmetry	Zero velocity normal to boundary

## 2.3 Grid Structure

In order to generate a suitable grid, the air volume is split longitudinally so that a shell containing structured hexahedral cells can extend along the entire length of the solution domain, situated above the two vehicles. This leaves a core region beneath the shell which is subdivided transversely into an upstream core placed

ahead of the towing vehicle and a downstream one located behind the trailer. This permits use of structured prism cells within these two core regions to minimise cell skewness. Grid stretching in the stream-wise and transverse radial directions ensures that the cell density increases in the vicinity of the remaining central core region, where flow gradients are expected to be highest. Stretching the grid in this way also keeps the cell count relatively low at 3.7 million cells within these shell and core regions (compared to tetrahedral cells, for example), see Figures 4(a) and (b).

Considerable care is taken in generating the grid in the remaining central core and cell refinement is limited to this volume for the purpose of a grid independence study, the results of which are described in section 3.1. A boundary layer mesh containing 12 layers of cells and a thickness of 0.08 m is wrapped around the primary surfaces of the trailer. With the exception of a thin boundary layer grid on the upper surface of the animals (see Figure 4(c)), all remaining space within the trailer and exterior to the vehicles is discretised using unstructured tetrahedral elements to deal with the geometric complexity. The size distribution of these cells is controlled by varying the surface grid spacing on the vehicles. This was progressively refined in three stages from an initial coarse spacing of 0.025 m to the fine spacing of 0.012 m, leading to global cell counts of 4.29 million and 8.07 million, respectively. The range of local grid structures in the vicinity of the front upper vent aperture is evident in Figures 4 (d)-(g). Grid generation was carried out using Gambit (version 2.6) (Ansys, 2015).

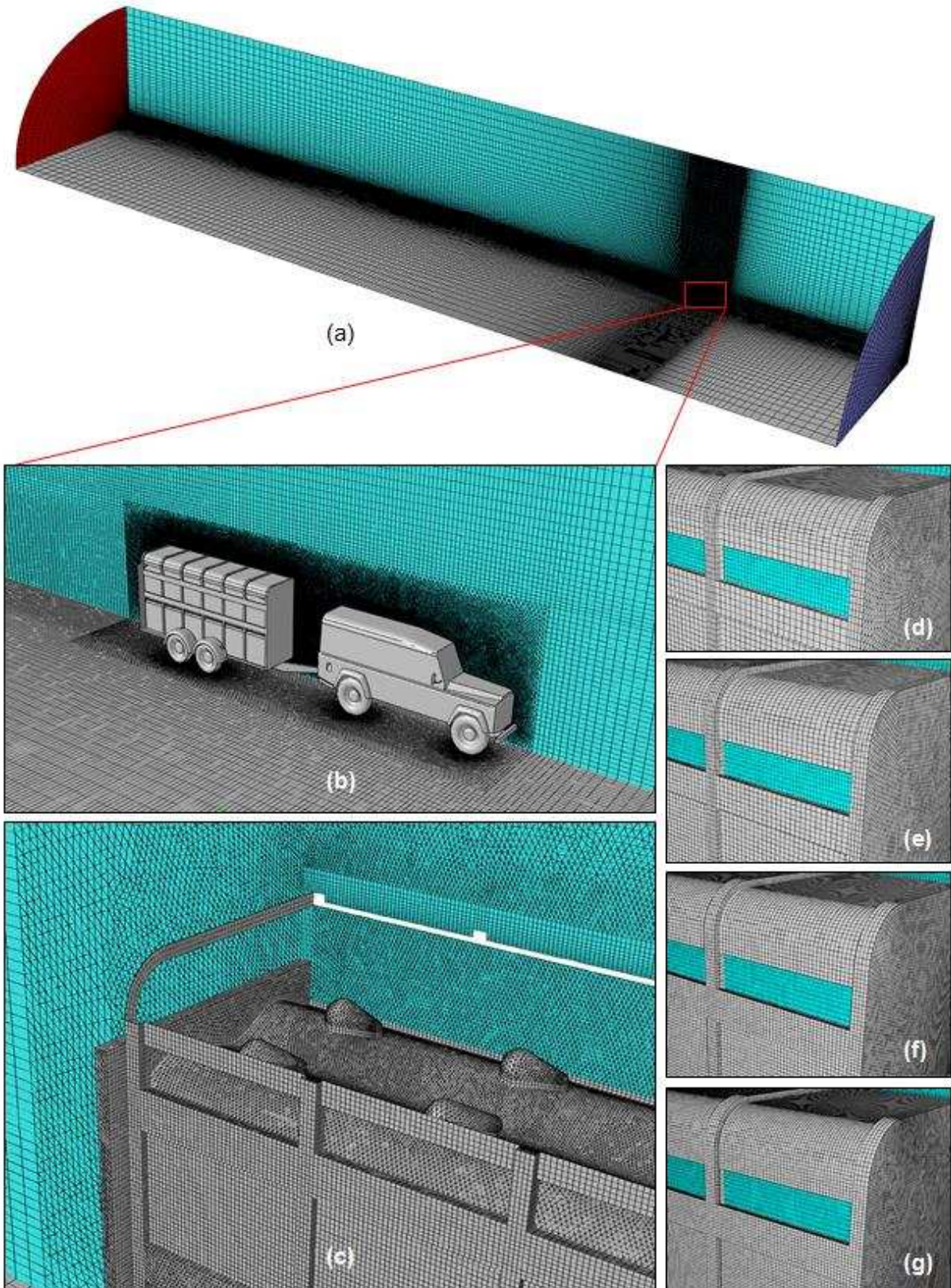


Figure 4: Grid structure of (a) the whole domain, (b) near both vehicles, (c) rear of the trailer showing upper deck of animals (with roof removed for clarity) and close-up views of (d) coarse, (e) medium, (f) fine and (g) extra-fine grids.

## 2.4 Numerical Schemes and Solution Strategy

The three dimensional governing - Navier-Stokes equations for isothermal fluid flow are represented by the conservation of mass,

$$\frac{\partial \rho}{\partial t} + \nabla \cdot \mathbf{u} = 0, \quad (1)$$

and the conservation of momentum in each of the three Cartesian coordinate directions, namely:

$$\frac{\partial(\rho u)}{\partial t} + \nabla \cdot (\rho \mathbf{u} u) = -\frac{\partial p}{\partial x} + \nabla \cdot (\mu \nabla u) + S_{M_x}, \quad (2)$$

$$\frac{\partial(\rho v)}{\partial t} + \nabla \cdot (\rho \mathbf{v} u) = -\frac{\partial p}{\partial y} + \nabla \cdot (\mu \nabla v) + S_{M_y}, \quad (3)$$

$$\frac{\partial(\rho w)}{\partial t} + \nabla \cdot (\rho \mathbf{w} u) = -\frac{\partial p}{\partial z} + \nabla \cdot (\mu \nabla w) + S_{M_z}, \quad (4)$$

where  $u$ ,  $v$  and  $w$  are the velocities in  $x$ ,  $y$  and  $z$  coordinate directions respectively,  $\rho$  is the fluid density,  $t$  is time,  $\mathbf{u}$  is the velocity vector,  $\mu$  is the dynamic viscosity and  $S_{M_x}$ ,  $S_{M_y}$  and  $S_{M_z}$  represent the momentum source terms in the  $x$ ,  $y$  and  $z$  coordinate directions respectively. The incompressible steady-state solutions to these were computed using the commercial CFD package, Fluent (version 6.3.26) (ANSYS, 2015). For a low vehicle speed of 4.47 m/s (10 mph) the Reynolds number,  $Re$ , is calculated to be  $2.9 \times 10^6$  which implies a turbulent flow regime requiring a turbulence model in computing the flow field. The Spalart Allmaras model (Spalart and Allmaras, 1992) was used for this purpose as it has been shown to produce accurate results when validated against wind tunnel experiments of a 1:7 scale livestock trailer (Gilkeson *et al.* 2009). The model solves one transport equation for the modified turbulent viscosity,  $\mu_t$ . The SIMPLE pressure-velocity coupling algorithm (Patankar and Spalding, 1972) was selected together with second order discretisation for the pressure equation and the QUICK scheme (Leonard 1979) for both the momentum equation and the transport equation for  $\mu_t$ . Computations were carried out for a total of 10,000 iterations and convergence of all quantities was observed after 9500 of these for the finest grid; this ensured that no inaccuracies were present in the solution, generated through lack of convergence. Typically, each converged solution produced absolute residual levels of  $10^{-5}$  for continuity,  $10^{-8}$  for momentum and  $10^{-6}$  for  $\mu_t$ . Double precision real number representation ensured that round-off error was minimised. Simulation times for solutions obtained on the finest grid ranged from 24 hours on 24 processors to 72 hours on 4 processors using a Beowulf high performance computing (HPC) cluster with a total of 32 AMD Opteron 64-bit, 2.4GHz processors, each with 2GB of RAM available.

### 3. Results

Following the description of the numerical methodology in section 2, a grid independence study is essential to determine a suitable grid density for further computations. This is discussed in section 3.1 followed by a brief correlation exercise to compare the results with validated CFD results (Gilkeson *et al.*, 2009). Sections 3.3 and 3.4 describe various methods for quantifying passive ventilation before investigating the impact of vehicle speed on ventilation rates.

#### 3.1 Grid Independence

Implementing rigorous verification and validation (V&V) procedures is important if accurate and reliable CFD simulations are sought (Roache, 1994; ERCOFTAC, 2000; AIAA, 2002; ASME, 2009). ERCOFTAC (2000) describes verification as the “procedure to ensure that the program solves the equations correctly” and this can be checked by carrying out a grid independence study. Figure 4 shows the four grid sizes considered, the statistics for which are displayed in the second and third columns of Table 2. As the local surface grid spacing on the trailer is refined, the cell count almost doubles from the coarse to the extra-fine grid. Although it is recommended that a constant grid refinement ratio is employed (Roache, 1994; ERCOFTAC, 2000; AIAA, 2002; ASME, 2009), in practice this was difficult to achieve at the mesh generation stage; skewness issues (particularly for the coarser grids) dictated the local grid spacing in each of the four grid structures. Despite this, the grid refinement ratio,  $r$ , varies between 1.25 and 1.33 which, in terms of magnitude, is in accordance with recent recommendations (ASME, 2009). As a reminder, cell refinement was only applied to the core volume which surrounds both vehicles. Here, the cell count actually rose sevenfold from an initial 0.6 million cells (coarse grid) to 4.3 million cells (extra-fine grid). Note that an empty trailer was used for the grid independence study; the animals were added for later simulations.

Table 2: Grid statistics and calculated flow rates through the lower deck of the trailer,  $Q_L$ , and the upper one,

$Q_U$ , at a vehicle speed of 22.35 m/s.

Grid Type	Local Grid Spacing (m)	Global Cell Count	$Q_L$ (m <sup>3</sup> /s)	$Q_U$ (m <sup>3</sup> /s)
Coarse	0.025	4290819	0.3420	1.2509
Medium	0.020	5207258	0.3632	1.2645
Fine	0.015	6669465	0.3605	1.2643
Extra-Fine	0.012	8076558	0.3646	1.2847

Simulations were run using each grid for a vehicle speed of 22.35 m/s (50 mph) and the flow rate,  $Q$ , through the trailer was calculated in the vent apertures. The variation in flow rate on the lower deck,  $Q_L$ , and the upper deck,  $Q_U$ , as a function of grid size is also shown in Table 2. Computations on all four grids yield similar flow rates through both decks, however, the flow direction in two of the vent apertures for the coarse grid solution did not match those obtained from the three finest grids, which were all in agreement. This explains the 6.2% discrepancy in  $Q_L$  between the coarse and medium grid solutions. The percentage difference between fine and extra-fine grid solutions is 1.2% and 1.6% for  $Q_L$  and  $Q_U$ , respectively. Such comparatively small discrepancies indicate that fine-grid solutions offer the best compromise between accuracy and the time required per simulation. Ideally, the Grid Convergence Index (GCI) (Roache, 1994) should be used to estimate the discretisation error because it considers the local grid spacing, the order of discretisation and the solution (per grid). The use of GCI is, however, only valid for constant grid refinement ratios which could not be achieved here, as described above. Nevertheless, the level of grid refinement employed is satisfactory (ERCOFTAC, 2000; AIAA, 2002, ASME, 2009). Consequently, the fine grid spacing of 0.015 m is applied to the surface of the vehicles in subsequent simulations. Furthermore, the animal shapes shown in Figure 2(c) are added, with cell refinement of 0.005 m applied to the muzzles, increasing the global cell count to 7630546.

### 3.2 Comparison with Validated Numerical Results

There are no experimental results available to validate the numerical results described for the full-scale problem above, however, the same numerical methodology was used in an earlier study to validate against open-return wind tunnel data for a 1/7<sup>th</sup> scale model of a generic towing vehicle and livestock trailer, at a Reynolds number of  $1.74 \times 10^6$  (Gilkeson *et al.*, 2009). Key features of this earlier validation study are presented here, before making comparisons to the full-scale results. The purpose of this is to highlight the similarities in flow structure and to provide basic indications of the accuracy of the underlying CFD methodology. Figure 5 shows experimental measurements of the normalised velocity distribution spanning the rear vent aperture with comparison to an equivalent CFD simulation, using the Spalart Allmaras turbulence model (Spalart and Allmaras, 1992). The velocity is normalised with respect to the free-stream velocity (19.2 m/s) measured immediately upstream of the working section,  $y$  is the distance measured from the left side of the vent opening and  $W$  is the width of the trailer (0.28 m). Although there is scatter in the experimental readings, the CFD results show good agreement, implying that the internal velocity field is well-predicted (Gilkeson *et al.*, 2009).

Furthermore, the pressure coefficient,  $C_p$ , is a convenient parameter to show the external pressure distribution around the trailer. Figures 6(a) and (b) show the horizontal stream-wise pressure distribution

adjacent to the lower and upper deck vent apertures respectively ( $x$  is the downstream distance measured from the trailer headboard and  $L$  is the length of the trailer which is 0.5 m for this model scale). The CFD pressure distributions broadly follow those of the experiments with the exception of the farthest downstream measurement location (Figure 6(b)). A similar comparison is evident for the pressure distribution on the roof of the trailer, highlighted in Figures 6(c) and 6(d) (note that the outboard profile is midway between the vehicle centerline and its left edge). Finally, base pressures are compared at two heights on the tailboard with good agreement between CFD and experiment for the lower profile, however, outboard measurements on the upper profile (Figure 6(f)) highlight a notable discrepancy. More details can be found in (Gilkeson *et al*, 2009).

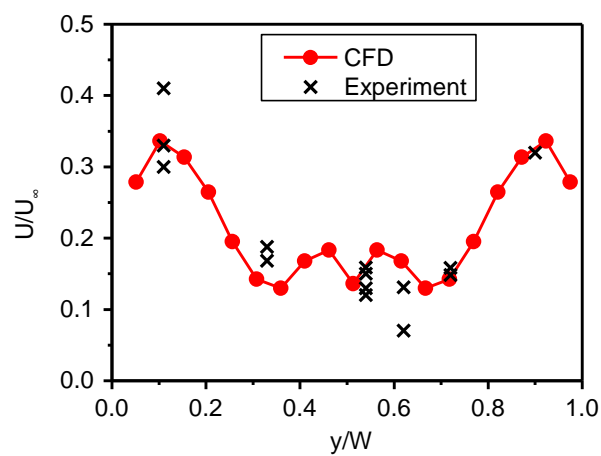


Figure 5: Comparison of experimental and CFD results of the normalised span-wise velocity distribution (Gilkeson *et al*, 2009)

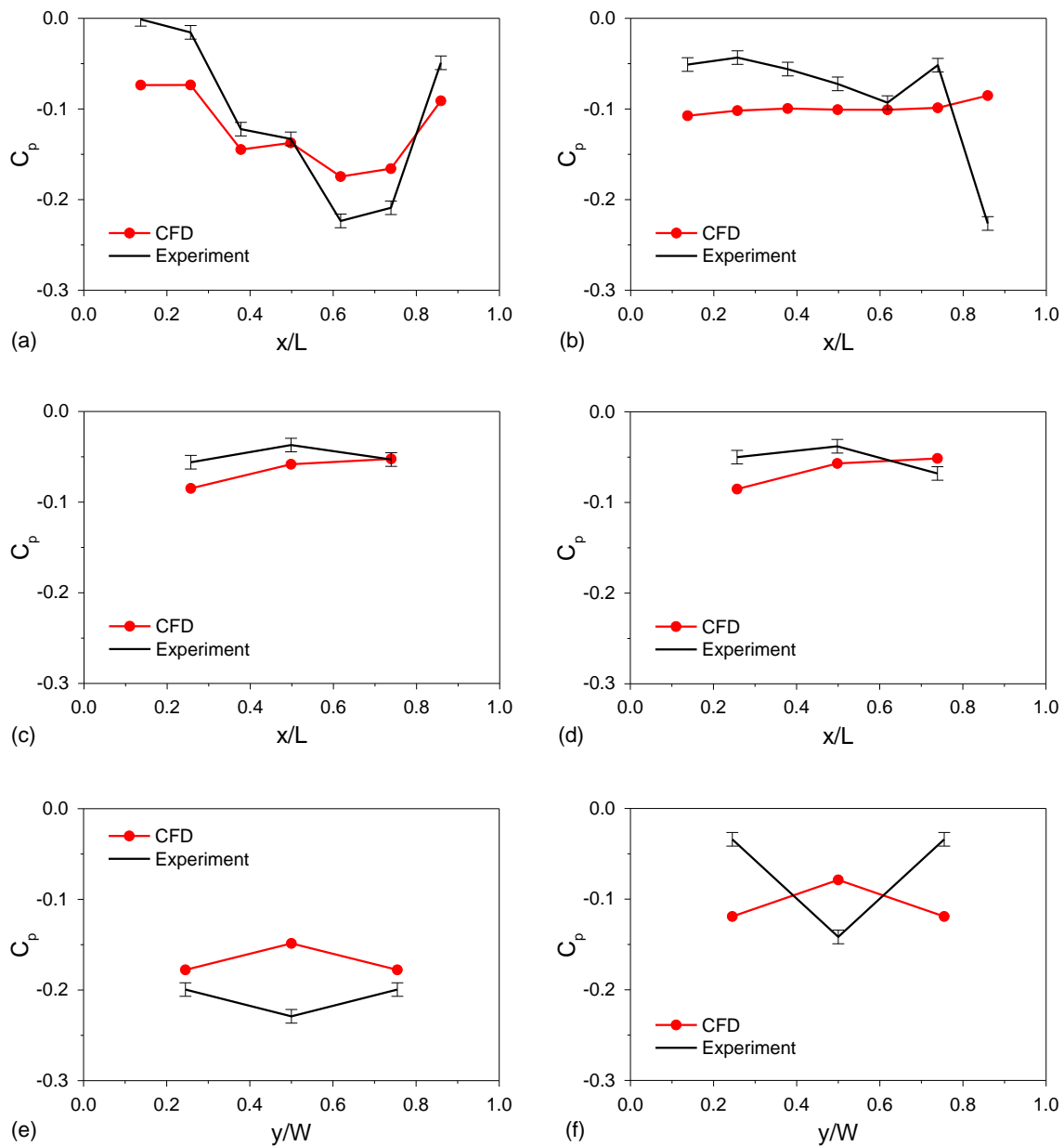
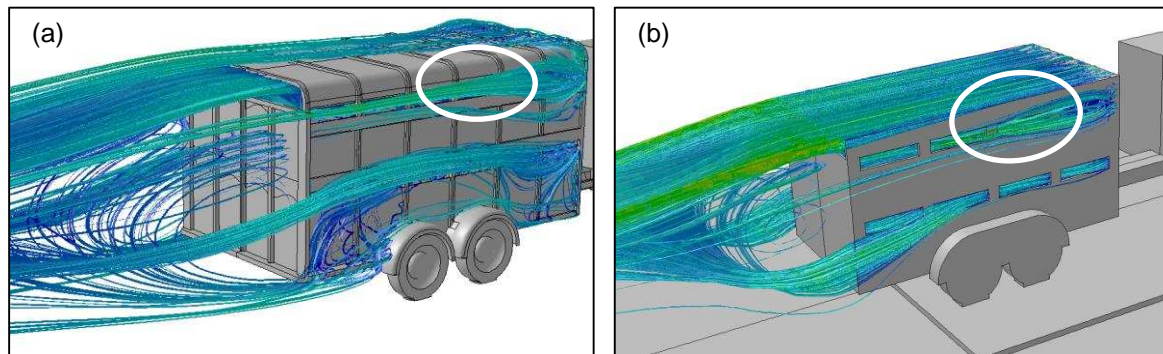


Figure 6: Comparison of experimental and CFD measurements of the pressure coefficient,  $C_p$ , along the: (a) lower and (b) upper deck; roof pressure profiles: (c) outboard and (d) centerline. Tailboard pressure profiles: (e) lower and (f) upper deck.

### 3.2.1 Qualitative Comparison

Figure 7 shows the similarity in airflow structure around the detailed and model scale vehicles. As described in section 2.2 the detailed geometry is assumed to be in free-air with a moving ground plane and rotating wheels which are representative of real operating conditions. In contrast, the scale model includes a stationary ground board to elevate the vehicles above the boundary layer of the wind tunnel floor, as per

the wind tunnel experiments (Gilkeson *et al.*, 2009). Furthermore, all walls are assumed to be stationary and the entire wind tunnel is modelled, restricting the advancing free-stream with a blockage of 3.4%. Despite the differences in scale and blockage, both airflow patterns are visually similar around the upper deck, with low-pressure suction regions present around the foremost upper vents (circled) and subsequent ingestion into the side vents further downstream. In both cases, extraction through the rear tailboard vent is pronounced.



*Figure 7: Pathlines generated from seeds released in the vent apertures of (a) the detailed full-scale trailer (free-air) and (b) the simplified scale model (wind tunnel).*

On the lower deck, a column of air exits the trailer in both cases but the point of exit is much further upstream for the detailed trailer case, see Figure 7(a). This difference is attributable to the fact that the trailer is wider than the towing vehicle, thereby exposing the lower portion of the bluff headboard to the free-stream, thus inducing low-pressure flow separation leading to the extraction seen. For the simplified, model-scale case the trailer is the same width as the towing vehicle which essentially shields the headboard from the free-stream, thus preventing flow separation adjacent to the front vents.

Extending the comparison to the interior of the trailer, normalised velocity magnitude contour plots are visually similar for both cases, as shown in Figure 8. Air velocities are below 10% of the free-stream value throughout the lower deck with higher velocity jets entering the downstream side vents on the upper deck. This underlines the similarity in flow conditions on the upper deck and the differences on the lower deck occur due to the differences in vehicle width, cited above.

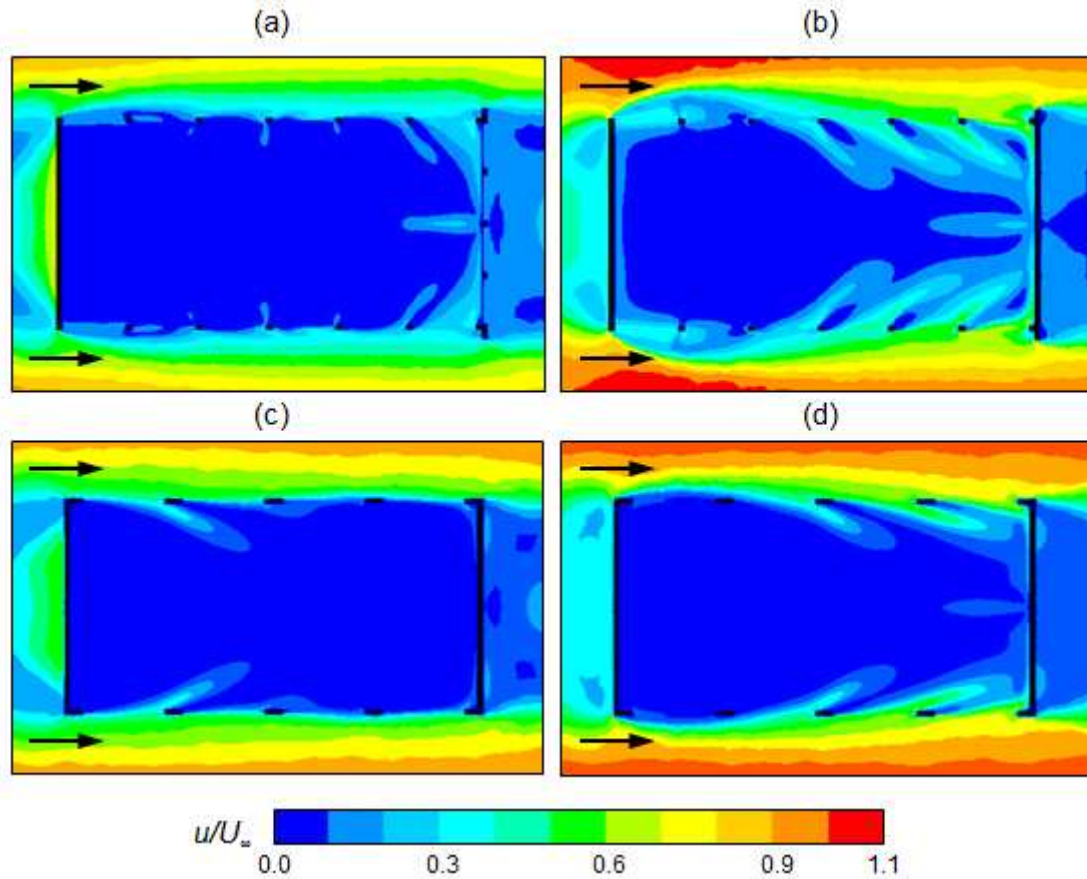


Figure 8: Aerial views of normalised velocity magnitude contour plots of (a) the lower vent plane, detailed geometry, (b) upper vent plane, detailed geometry, (c) lower vent plane, simplified geometry and (d) upper vent plane, simplified geometry. Arrows indicate the free-stream flow direction, which is from left to right

### 3.2.2 Quantitative Comparison

Quantitative comparisons are made in Table 3. The drag coefficient,  $C_D$ , for the detailed geometry is 23% less than that of the simplified one, which is attributable to the rounding present on many of the edges of the towing vehicle, the trailer roof and the wheels. These are features of real vehicles which the detailed geometry is modelled on, whereas the simplified wind tunnel model has sharper edges. In order to compare ventilation rates at different scales, the ventilation coefficient,  $C_V$ , was proposed by Gilkeson *et al.*, (2009) and is given by,

$$C_V = \frac{t}{t_{REG}}, \quad (5)$$

where  $t$  is a dimensionless time parameter, namely,

$$t = \frac{TU_\infty}{L_S}, \quad (6)$$

with  $T$  being the time taken for a single air exchange, found from the computed flow rate through each trailer deck,  $U_\infty$  is the free-stream velocity and  $L_s$  is the scale of the simulation, see Table 3. Similarly,  $t_{REG}$  is calculated from,

$$t_{REG} = \frac{T_{REG} U_\infty}{L_s}, \quad (7)$$

where  $T_{REG}$  is the time taken for an air exchange in full-scale livestock trailers based on the regulatory ventilation rate of 60 m<sup>3</sup>/h/kN of animal liveweight specified by European Union Council Regulation (EC) No. 1/2005 (European Union, 2005): note that this regulation document remains current and must be adhered to. The lower the ventilation coefficient, the higher the ventilation rate. For  $0 < C_v < 1$  the ventilation rate exceeds the regulations, if  $C_v = 1$  the regulations are satisfied and for  $C_v > 1$  this denotes that ventilation is below the regulatory limit.

Observing the results comparison of  $C_v$  in Table 3, in both cases the ventilation coefficient on the upper deck,  $C_{vU}$ , exceeds the regulatory threshold, whereas it is below this value on the lower deck (also in both cases). The results presented in this section highlight the fact that the CFD simulations based on the detailed full-scale livestock trailer are broadly similar to the validated simulations of the simplified scale model, giving a reasonable degree of confidence in the accuracy of the full-scale simulations, which are the subject of the remainder of this paper.

*Table 3: Comparison of drag and ventilation characteristics obtained for the simplified and detailed vehicles.*

Simulation Layout	$L_s$	$U_\infty$	$Re$	$C_D$	$C_{vL}$	$C_{vU}$
Simple scale-model vehicle (wind tunnel)	1/7	19.2	$1.70 \times 10^6$	0.714	1.366	0.304
Detailed full-scale vehicle (free-air)	1	17.9	$1.16 \times 10^7$	0.538	1.157	0.617

### 3.3 Pressure Distribution and Airflow Structure

Numerical simulations of airflow around the full-scale towing vehicle and livestock trailer were carried out for the five aforementioned vehicle speeds ranging from 4.47 m/s (10 mph) to 22.35 m/s (50 mph). The drag coefficient remains constant at 0.54 (to two decimal places) for all velocities which is expected given the high Reynolds numbers. Of the total drag force, 37% is attributable to the towing vehicle with the remaining 63% acting on the trailer further downstream. Considering the distribution of drag acting on the trailer only, the headboard contributes the greatest proportion with 48% of the trailer total, 31% is due to the tailboard

with the remaining 21% attributable to the underbody components, roof and side panels. The dominant contribution from the headboard is partly because of the upper stagnation region which occurs due to the 0.32 m of extra height of the trailer, compared to the towing vehicle. The resulting peak pressure coefficient on the headboard is around 0.8 as indicated by the pressure distribution in Figures 9(a) and (b) for the medium vehicle speed of 13.4 m/s; the pressure coefficient distribution practically is the same for all five air velocities. This is expected due to the incompressible nature of the flow at these velocities where the Mach number range is only 1.3-6.6%, and significantly below the limitation of incompressibility.

The  $C_p$  plot in figure 9(c) compares the longitudinal profiles along three sections of the trailer. Sections A-A and B-B indicate the pressure distributions in the vicinity of the lower and upper vent apertures, respectively. Section A-A is positioned 0.06 m above the lower vent apertures with section B-B 0.06 m below the upper vent apertures. Section C-C considers the centerline distribution along the roof. All three profiles show negative pressure coefficients near the front of the trailer which is indicative of low-pressure suction, due to local flow separation. Moving further downstream, pressure recovery is evident with observed pressure coefficients in the range of -0.15 to -0.05, at approximately half-way along the trailer ( $x/L_T = 0.5$ ). This pressure recovery is further enhanced at the rear of the trailer due to stagnation on the tailboard which protrudes sideways into the free-stream, thereby locally increasing  $C_p$  above zero.

As a consequence of the suction at the front of the trailer, air from within both decks is extracted through the upstream vent apertures. This is clear in Figure 10 which illustrates the airflow patterns from seeds released within the vent apertures. However, moving further downstream, the observed flow patterns differ considerably between the two decks. This is more easily revealed from contour plots of the relative velocity magnitude within the trailer as shown in Figure 11, which is also shown for the medium vehicle speed of 13.41 m/s. Here, horizontal contour plots are compared in two planes, one per deck, each taken at the mid-height of each respective row of vent apertures. The overlaid arrows indicate the flow direction in locations of interest. Although the air velocities are significantly reduced compared to the free-stream value, in terms of ventilation, the upper deck benefits from air jets entering the trailer through the four downstream vent openings. This incoming fresh air then passes through the rear tailboard vent which presents a clear route to the low-pressure wake region; this mechanism is not present in the lower deck as there is no rear vent at this level. An interesting feature of the airflow in the centre of the lower deck is that it opposes the free-stream as indicated by the two white arrows in Figure 11(a). This is explained by the extraction of air through the upstream vent, coupled with the ingestion through the furthest downstream vent. This induces a circulatory flow field with air adjacent to the vents moving downstream and air in the centre of the trailer moving in the opposite direction.

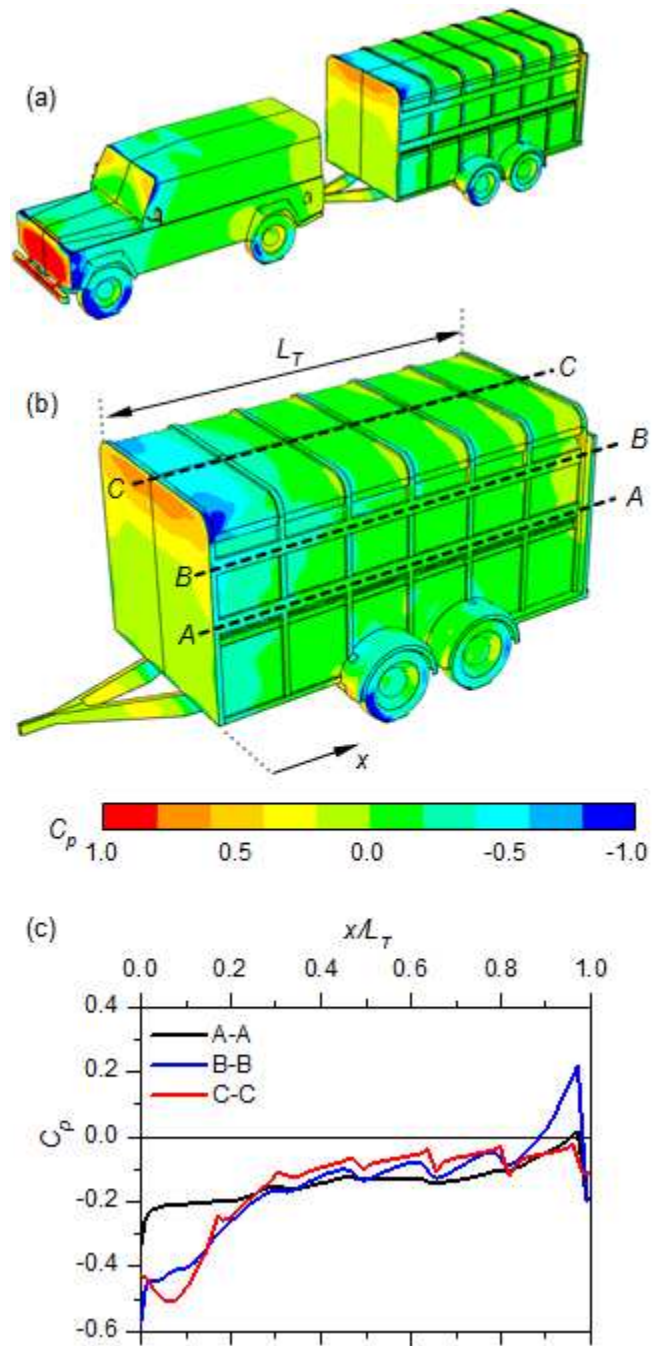


Figure 9: Contour plots of the pressure coefficient ( $C_p$ ) distribution on (a) both vehicles, (b) the trailer and (c) longitudinal  $C_p$  profiles at sections A-A, B-B and C-C as indicated in (b).  $U_\infty = 13.41$  m/s.

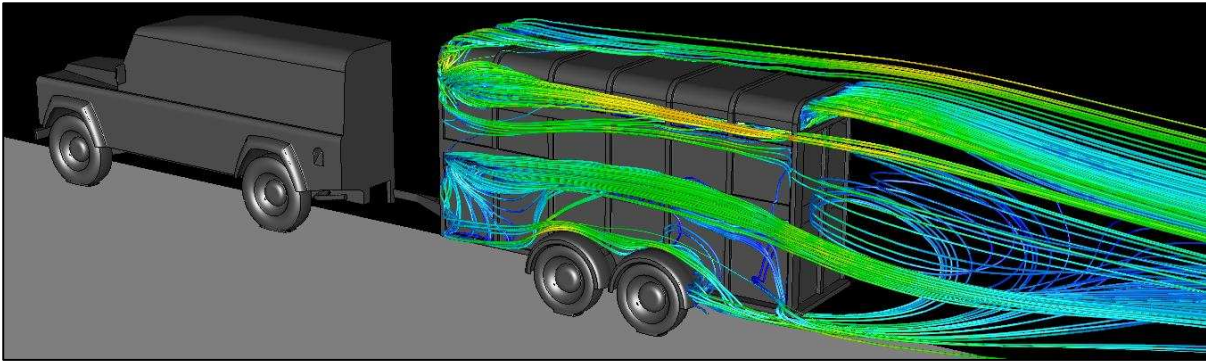


Figure 10: Pathlines showing airflow patterns around the livestock trailer generated from seeds released in the vent apertures.

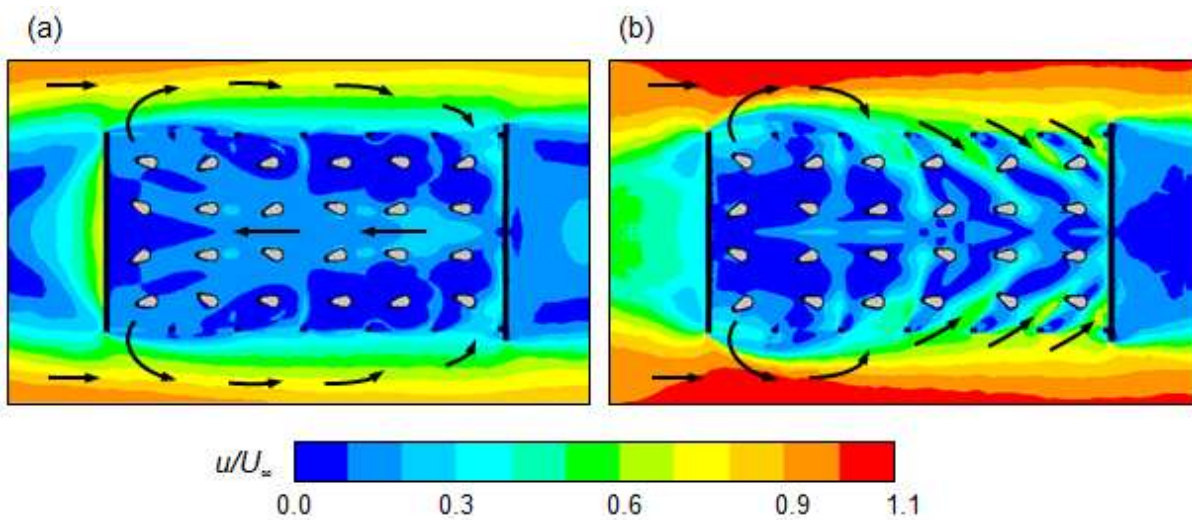


Figure 11: Aerial view of the relative velocity magnitude contour plots through (a) the lower vents and (b) the upper vents at a free-stream velocity,  $U_{\infty} = 13.41$  m/s. The flow direction is from left to right

### 3.4 Quantifying Ventilation

Whilst the information presented in figures 9-11 provides useful insight into the complex flow fields, adequately quantifying the ventilation rates is of greater importance from the animal welfare perspective. This sub-section summarises three differing approaches to this.

#### 3.4.1 Method 1: Flow Rates

The most straightforward method for quantifying ventilation is to consider the volumetric flow rates measured through the vent apertures as these openings act as the inlets and outlets to each respective deck.

Figure 12 shows the vent aperture flow rates, expressed in  $\text{m}^3/\text{minute}$ , for the intermediate vehicle speed of  $13.41 \text{ m/s}$ . The relative contribution of air exchange rates seen is representative of the five speeds considered. Of the total air volume flowing through the trailer, twice as much flows through the upper deck compared to the lower one. As a comparison, the results for the empty trailer simulations (i.e. without animals present) are also shown. Although the presence of animals drastically reduces the available air volume within both decks of the trailer, the resulting flow rates are broadly the same with notable differences only evident around vent numbers 2, 3, 7 and 10. However, these local differences are insufficient to alter the overall flow patterns which are essentially the same.

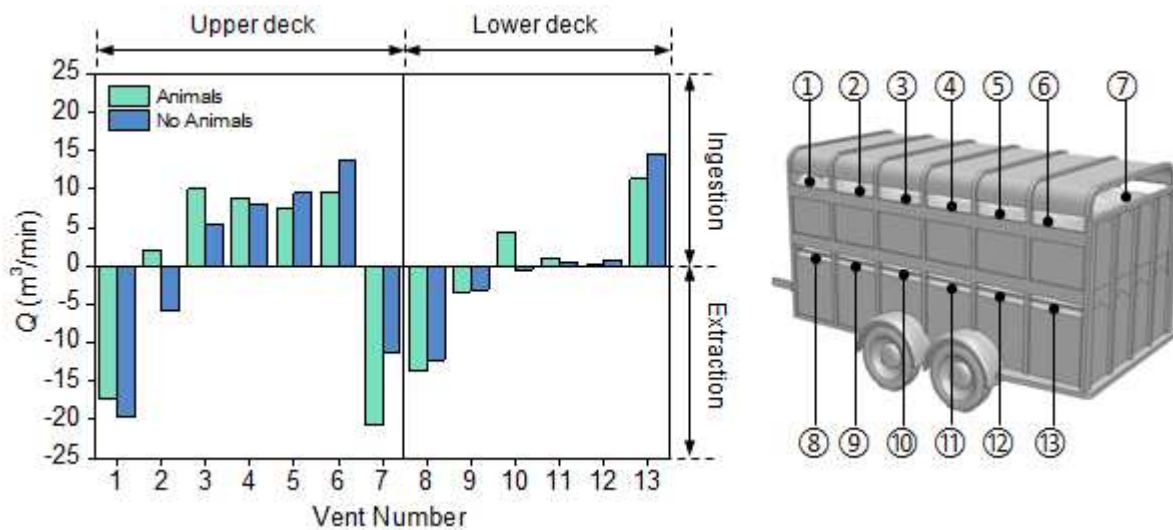


Figure 12: Volumetric flow rates through the vent apertures for  $U_{\infty} = 13.41 \text{ m/s}$ .

Focussing on the trailer loaded with animals, it is clear that greater air movement is present on the upper deck with notable extraction through vent 1 and the rear tailboard opening, vent 7. Fresh air enters the remaining openings in this deck of the trailer, vents 2-6, as depicted from the aforementioned jets highlighted in Figure 11(b). On the lower deck, extraction is also evident in the upstream opening, vent 8, and to a lesser degree, through vent 9. Moving further downstream, the air exchange rates are small, particularly through vents 11 and 12 which is coincident with the low pressure gradient in this region, indicated by section A-A in the horizontal location range of  $0.4 < x/L_T < 0.8$  in Figure 9(c). A significant amount of ingestion occurs through the rear opening, vent 13, which drives the back-to-front flow direction in the heart of the trailer shown in Figure 11 (a).

To put these results into perspective, the ventilation coefficient described in section 3.2.2 provides a convenient metric to compare ventilation effectiveness at the five vehicle speeds considered. As the geometry of interest is full-scale, the ventilation coefficient simplifies to:

$$C_V = \frac{T}{T_{REG}} \quad (8)$$

Recalling that  $T$  is the time taken for a single air exchange; this can be deduced from the net volumetric airflow rate entering (or exiting) the trailer, in each deck, depending on the free-stream velocity. Similarly,  $T_{REG}$  is determined from the regulatory flow rate for this class of trailer which was previously defined as 60 m<sup>3</sup>/h/kN of animal liveweight (European Union, 2005). Given the maximum payload of 3500 kg for this specific trailer, the maximum liveweight is 34.335 kN which leads to the requirement of 1030 m<sup>3</sup>/h (0.2861 m<sup>3</sup>/s), per trailer deck, assuming equal liveweight in each. Dividing this regulatory flow rate by the volume in each deck leads to the time required for one air exchange,  $T_{REG}$ . With available air volumes of 0.64 m<sup>3</sup> and 1.01 m<sup>3</sup> on the lower and upper decks, respectively, the associated values of  $T_{REG}$  are 2.24 s for the lower deck and 3.54 s for the upper one. Based on the volumetric flow rates determined in each deck for the full range of vehicle speeds, the ventilation coefficients are calculated and plotted in Figure 13.

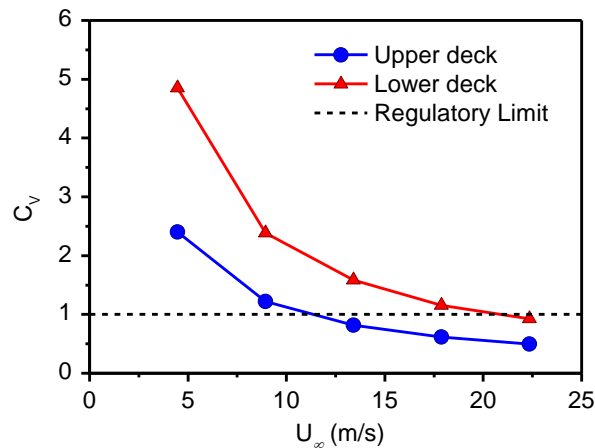


Figure 13: Plot of the ventilation coefficient,  $C_V$ , as a function of the free-stream velocity,  $U_\infty$  (Satisfactory ventilation corresponds to  $0 < C_V < 1$ ).

Recall that in order to satisfy the regulations, ventilation coefficients of 1 or below are desirable. Clearly this is not achieved in the lower deck other than for the highest air velocity of 22.35 m/s (50 mph). This is partly because the small pressure gradient in the vicinity of vents 9-12 renders them ineffective and so less air flows through this deck of the trailer. However, significant improvement is seen on the upper deck with ventilation rates satisfying the regulations for the three highest free-stream velocities. Again there is an issue at lower velocities, however, the ventilation coefficient is approximately half that of the lower deck, owing to the improved flow through the trailer, as depicted in Figure 11(b).

### 3.4.2 Method 2: Passive Scalar Residence Times

Method 1 is effective at quantifying how well-ventilated the trailer is, however, it does not consider flow behaviour beyond the vent apertures which are on the perimeter of each deck. To understand flow behaviour deeper within the interior of the trailer, a convenient solution is to obtain the distribution of residence time,  $T_R$ , which is a measure of how long it takes the air to refresh once in each computational cell within the domain, assuming steady-state conditions. This is achieved by solving an additional passive scalar transport equation, with a low scalar diffusivity of  $1 \times 10^{-6}$  kg/ms and source terms applied in each deck. The approach is analogous to releasing a coloured dye in a stream of water to highlight how quickly the flow is moving from the observed dye concentration. By setting source terms within each trailer deck (only), the scalar concentration depends on the local air velocity and is directly related to  $T_R$ , which enables contours plots of the residence time to be determined. The low diffusivity ensures that the scalar is transported via advection of the airflow only. This approach has been used in another study to calculate ventilation effectiveness in hospital wards (Short *et al.*, 2014).

Accordingly, the scalar transport equation was solved using 2<sup>nd</sup> order discretisation for each vehicle speed. The flow equations were deactivated to ensure that the resulting residence time (scalar) distribution corresponds to the converged steady-state flow fields already analysed. Each scalar solution converged in approximately 50 iterations. Figure 14 highlights the resulting residence time distribution on the surfaces of the animals and at 7 equally spaced vertical planes within the trailer, for the slowest velocity of 4.47 m/s.

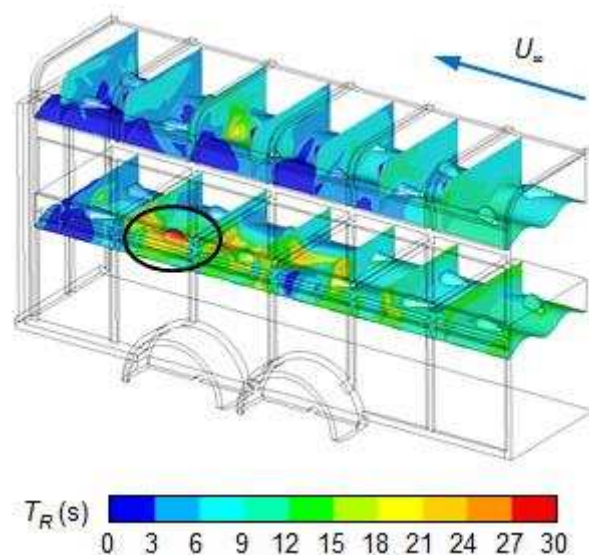


Figure 14: Contour plots of residence time,  $T_R$ , viewed inside the trailer on the upper surfaces of the animals and a series of vertical planes at a vehicle speed of 4.47m/s.

Clearly the air takes longer to refresh in the lower deck, especially for the animal adjacent to vent 12 (circled) with an associated residence time of approximately 30 seconds. In terms of animal welfare, the residence times occurring in the two horizontal breathing planes are of particular interest, with each one passing through the mean animal head height per deck. Furthermore, by replacing  $T_r$  for  $T$  in equation (8), a new residence time ventilation coefficient,  $C_{VR}$ , can be calculated to present these residence times in terms of the regulatory ventilation rate stated previously. Thus  $C_{VR}$  is given by:

$$C_{VR} = \frac{T_R}{T_{REG}} \quad (9)$$

Figure 15 shows the distribution of  $C_{VR}$  in both breathing planes for the full range of vehicle speeds considered. In essence, these plots are ventilation maps which indicate where the regulations are satisfied.

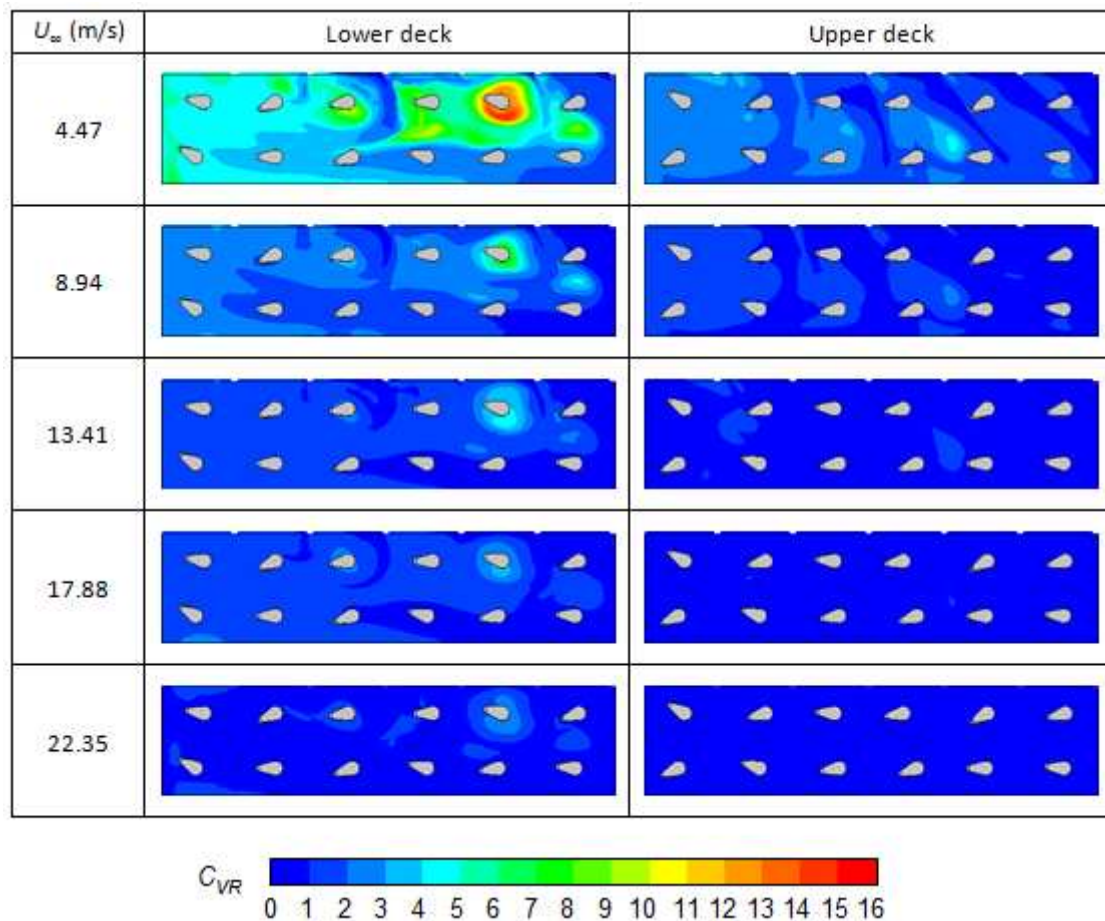


Figure 15: Breathing plane contour plots of the ventilation coefficient based on residence time,  $C_{VR}$ , as a function of free-stream velocity and location. Free-stream flow direction is left-to-right, upper edges denote location of vent apertures, lower edges denote symmetry plane location.

As expected, the general trend is for  $C_{VR}$  to reduce as the free-stream velocity increases and thus the local ventilation rates increase. Again, ventilation is notably better on the upper deck whereas comparatively little air movement on the lower deck leads to correspondingly high residence times and ventilation coefficients. This comparison is clearer in the plot of the average  $C_{VR}$  value in each breathing plane against  $U_\infty$ , see Figure 16(a). Note that the resulting ventilation coefficients are comparable to, but slightly less, than those previously calculated from the volumetric flow rates ( $C_V$ ) through the vent apertures (method 1). With the focus being that of animal welfare, the local ventilation coefficient in the vicinity of the animal muzzle (mouth region) is particularly important. Accordingly, a parameter termed the percentage of animals satisfactorily ventilated (PASV) is introduced which quantifies how many of the animals experience satisfactory ventilation at the muzzle, see Figure 16(b). The criterion for satisfactory ventilation is for the regulatory ventilation rate to be achieved such that  $C_{VR} \leq 1$ . Only on the upper deck does this occur for every animal, at the two greatest vehicle speeds. None of the animals experience satisfactory ventilation at the slowest velocity of 4.47 m/s, however, the situation improves with increasing velocity (in both decks).

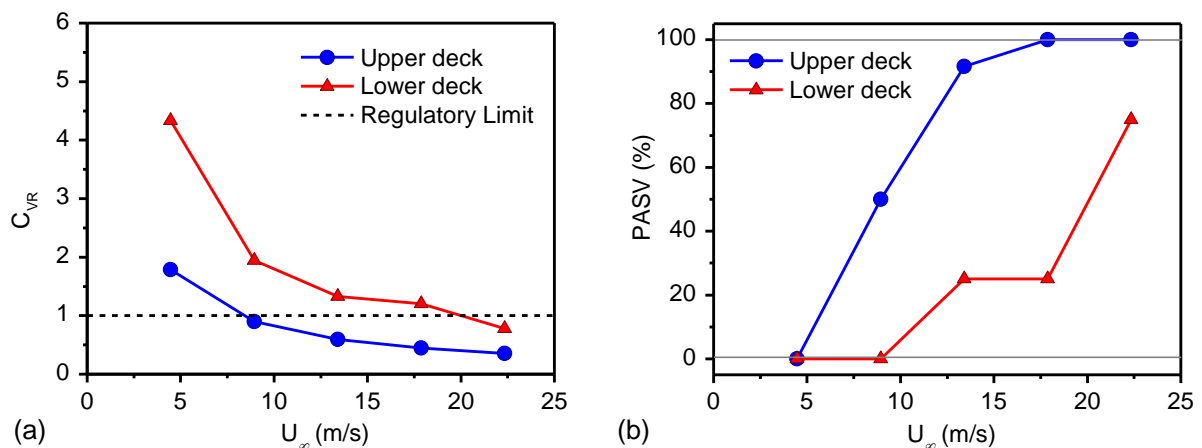


Figure 16: Plots of (a) the residence time ventilation coefficient,  $C_{VR}$  and (b) the percentage of animals satisfactorily ventilated, PASV, as a function of the free-stream velocity,  $U_\infty$  (Satisfactory ventilation corresponds to  $0 < C_{VR} < 1$ ).

### 3.4.3 Method 3: Residence Times from Muzzle-Point Particle Tracks

A different approach to determining ventilation effectiveness is to make use of particle tracking, releasing a massless 'seed' from each animal muzzle. Based on the air velocity in each computational cell, the path taken by each seed is then analysed and the cumulative time taken from release to trailer exit,  $T_p$ , can be calculated (Gilkeson *et al.*, 2009). In a similar fashion to methods 1 and 2,  $T_p$  replaces  $T$  in equation (8) to

produce a particle tracking based ventilation coefficient,  $C_{VP}$ , where the mean average value of  $T_p$  for all animals on a given deck is used. Thus  $C_{VP}$  is given by:

$$C_{VP} = \frac{T_P}{T_{REG}}. \quad (10)$$

Figure 17 shows the variation of  $C_{VP}$  with  $U_\infty$  along with equivalent plots for  $C_V$  (method 1) and  $C_{VR}$  (method 2).

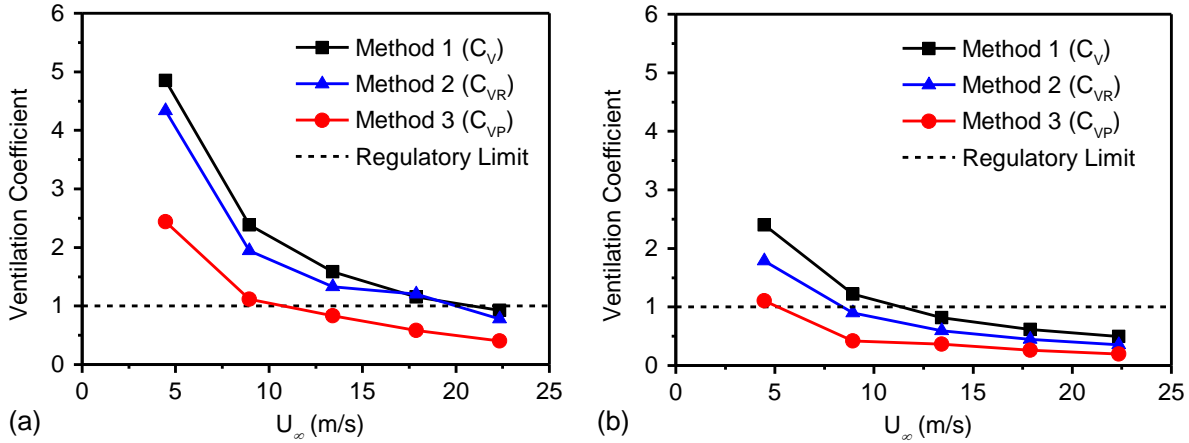


Figure 17: Plots showing the comparison between  $C_V$ ,  $C_{VR}$  and  $C_{VP}$  against  $U_\infty$  in (a) the lower and (b) the upper deck. (Satisfactory ventilation corresponds to  $0 < C_{VR} < 1$ ).

As with methods 1 and 2, method 3 yields the same trend of decreasing ventilation coefficient with increasing vehicle speed. Interestingly both  $C_{VP}$  plots suggest improved ventilation throughout the trailer compared to the more conservative results predicted by  $C_V$  and  $C_{VR}$ . The regulatory ventilation rate is almost entirely satisfied for the full range of speeds considered; only on the lower deck, at the slowest velocity, is ventilation noticeably inadequate. However, even in this case, 4 out of 12 of the animals on this deck (for the half domain) experience adequate ventilation i.e.  $C_{VP} \leq 1$ . Three of these animals are in the vicinity of vent number 8 where the extraction rate is high. In contrast, the lack of air exchange through vent number 12 leads to the greatest residence time of 19.5 s at the muzzle point of the nearest animal (indicated by the circle in Figure 14). This corresponds to  $C_{VP} = 8.7$  which is the highest muzzle-point ventilation coefficient throughout the trailer.

It should be noted that method 3 considers ventilation efficacy at muzzle points only and these locations will inevitably move with everyday livestock transportation. Nevertheless, the distribution of muzzle points selected in the study provides adequate coverage within this type of livestock trailer. Furthermore, it is of no

surprise that method 2 predicts higher ventilation coefficients than method 3. This is because method 2 accounts for all regions of the trailer, within each respective breathing plane. Therefore, the observed stagnant regions serve to increase the average residence time and thus reduce predicted ventilation efficacy.

## **4. Discussion**

### **4.1 Modelling Approach**

The results from this investigation provide a detailed insight into the passive ventilation characteristics of small livestock trailers for a typical range of steady vehicle speeds. The numerical approach enabled the flow field to be examined in a level of detail which would be practically unattainable through experimental means. A key feature of the computational domain is the coupled nature of the airflow with the internal trailer environment directly connected to the external free-stream, through vent apertures. The orientation of these apertures is such that high flow gradients exist at the interface between internal and external regions during transit. Consequently this places high demands on the quality and density of the computational grid in these locations. A rigorous grid independence study overcame this challenge, providing assurance in the quality of the results, which, when compared with existing wind tunnel data (Gilkeson *et al.*, 2009), gave confidence that the correct flow physics was predicted. Furthermore, certain flow features such as the slow-moving airflow behind the headboard is consistent with observations from other livestock transporter vehicles (Dalley *et al.*, 1996; Hoxey *et al.*, 1996; Quinn and Baker, 1997; Purswell *et al.*, 2005; Warriss *et al.*, 2006).

### **4.2 General Ventilation Characteristics**

A common feature of flow patterns observed within livestock transporters in general, is that the air movement in the centre of the container is often back-to-front, opposing the free-stream (Hoxey *et al.*, 1996; Mitchell and Kettlewell, 2008). This is linked to the external surface pressure distribution typically consisting of low-pressure suction around upstream vents, which acts as a sink, extracting airflow from deep within the trailer. Further downstream, higher ambient pressure allows external airflow to enter the trailer before being pulled forward towards the upstream low-pressure region. This circulatory flow pattern is observed on the lower deck of the small livestock trailer considered in this study. Although the same suction mechanism is also present in the upstream portion of the upper deck, the internal flow patterns further downstream are somewhat different. The presence of a rear vent aperture provides a clear route for the incoming ventilation currents to exit the rear of the trailer, where the local static pressure in the vehicle wake has a natural tendency to be lower. As a result, the net flow rate and thus the ventilation rate through the upper deck is double that of the lower deck. Another aspect which contributes to the reduced

ventilation rate on the lower deck is the lack of a notable pressure gradient along a large portion of the trailer side panels; such a gradient is essential for promoting air exchange through the vent apertures (Hoxey *et al.*, 1996).

### 4.3 Quantifying Ventilation

One of the difficulties of quantifying ventilation in a passive, naturally-ventilated vehicle, is that the inlets and outlets are not as clearly defined as for a mechanically ventilated system. Instead, each vent opening typically has a mixture of flow entering and exiting the area depending on the local pressure gradient. The advantage of numerical modelling is that the flow structure in these critical areas can be examined in great detail. Three different methods were used to quantify ventilation, the first of which (method 1) considered volumetric flow rates measured through the vent apertures. This revealed that ventilation rates increase with the forward vehicle speed, however, the rate of increase reduces significantly above 20 m/s. The results indicate that ventilation rates would be constant at vehicle speeds greater than 25 m/s (refer to Figure 13).

Whilst ventilation rates are readily determined using method 1, of greater importance is whether these are actually sufficient. The ventilation coefficient (Gilkeson *et al.*, 2009) provides a means for ventilation rates to be normalised against the regulatory flow rate of 60m<sup>3</sup>/h/kN liveweight, based on EU legislation (European Union, 2005). Analysis of the flow rates obtained for the full range of vehicle speeds (4.47-22.35 m/s) indicate that the regulations are only satisfied at 22.35 m/s on the lower deck and for vehicle speeds in excess of 13.41 m/s on the lower deck. One issue with this method is that it relies on flow rates through vent apertures on the perimeter of each deck and it does not reveal flow behaviour deeper inside the trailer, where the animals are situated.

This prompted two further approaches to consider ventilation in targeted areas of interest: namely the passive scalar approach (method 2) and particle tracking (method 3). Both of these methods indicate that the average ventilation rates in the breathing plane and around animal muzzle points are significantly better than the conservative prediction of method 1, which relies on flow rates only. More importantly, the results highlight the *variation* of ventilation throughout these critical regions. Ventilation coefficient maps in the breathing planes (Figure 15) clearly illustrate which locations within the trailer may be susceptible to poorer ventilation, potentially impacting animal welfare. Unsurprisingly the area behind the headboard coincides with reduced ventilation rates, especially on the lower deck. Furthermore, the lack of air exchange through one of the downstream lower side vents adversely impacts ventilation for one particular animal; the absence of a pressure gradient in the vicinity of the nearest vent is cited as the main reason for this. A key observation from the particle tracking analysis is that the time taken from each muzzle point to trailer exit is

generally short and the air does not spend long recirculating within the trailer interior. Of the three approaches considered, method 1 gives the most conservative quantification of ventilation rate. It is for this reason that method 1 is probably the most suitable for use by policy makers; however, method's 2 and 3 do highlight the distribution of ventilation efficacy throughout the trailer and so these should not be overlooked.

#### 4.4 Suitability of Existing Legislation

Throughout this article, the regulatory ventilation rate of 60m<sup>3</sup>/h/kN liveweight has been cited as the basis for whether or not adequate ventilation is achieved in the trailer. This regulation is specified by EU Council Regulation 1/2005, Chapter XI, section 3.2 (European Union, 2005) and it is enforced in England by The Welfare of Animals Order 2006 (Anon, 2006) and through guidance issued by the Department for Environment Food & Rural Affairs (DEFRA, 2012). It is important to appreciate that this regulatory ventilation rate is aimed at large transport vehicles for journey times in excess of 8 hours and with a mechanical ventilation system in operation. There are no provisions for passively-ventilated, small livestock trailers which are designed for comparatively short journey times. This brings into question whether a separate regulation is necessary for this class of livestock transporter. Despite this, the above regulatory figure was extremely useful for putting the numerical results of this investigation into context and it provides a design target for any class of vehicle.

Though not relevant in this study, EU Council Regulation 1/2005 also specifies additional provisions for livestock vessels transported in sea containers with no ambient wind, under Chapter IV, section 1 (European Union, 2005). It is a requirement for such a transport vehicle to be equipped with a forced ventilation system capable of changing the air in its entire volume (i.e. the empty volume) by a minimum of 40 air changes per hour (ACH) for a vehicle height of up to 2.3 m. Given that the livestock trailer analysed in this paper is under 2.3 m high, the above requirement of 40 ACH can be used to evaluate its performance. For the purposes of this investigation, the air change rate,  $A$ , per deck, is given by:

$$A = \frac{V}{Q}, \quad (11)$$

where  $V$  is the internal air volume of the deck (m<sup>3</sup>) and  $Q$  is the volumetric flow rate (m<sup>3</sup>/h) of air passing through it. At the slowest vehicle speed considered, 4.47 m/s, the upper and lower decks experience 83 ACH and 42 ACH respectively, based on an empty trailer and the volumetric flow rates measured in the vent apertures (from method 1). What this illustrates is that even at the lower limit of the vehicle speeds considered, the trailer experiences sufficient passive ventilation during transit to satisfy the extreme requirements for forced ventilation in enclosed spaces with no ambient wind. This encouraging result does

suggest that the three variations of the ventilation coefficient proposed in this paper ( $C_V$ ,  $C_{VR}$  and  $C_{VP}$ ) are conservative and that ventilation effectiveness is achieved by the trailer design, even at the lower vehicle speed. However, animal welfare issues are likely to arise when the vehicle is either stationary or moving very slowly, for example in situations where road traffic and/or congestion may occur.

#### **4.5 Recommended Design Improvements**

The generic livestock trailer considered in this investigation is representative of the type of vehicle used to transport sheep, pigs and cattle within the United Kingdom. The design is based primarily on space requirements and so there is little scope to make changes which would encroach on the internal space. However, a non-intrusive design improvement would be to modify the lower portion of the tailboard to embed vent openings to promote greater air movement on the lower deck. Such a design change would replicate the improved flow structure seen on the upper deck and mitigate against potential welfare issues. One caveat would be for the vent design to have a closable/sliding flap because the tailboard also acts a ramp for loading animals into the trailer. It should be noted that this design suggestion is based on the particular type and size of trailer considered in this article. As such, the benefits of such a change may not produce the expected results for other trailer types, especially if the flow regime differs in this critical region.

Another idea involves retro-fitting a headboard fairing in the space available between the towing vehicle and the trailer. A separate numerical study (based on the same geometry considered in this paper) demonstrated the potential of this solution through an aerodynamic shape optimisation study (Gilkeson *et al.*, 2013). The results predicted an appreciable 5.3% reduction in aerodynamic drag, with a minor improvement in the heat stress experienced by sheep on the lower deck. One key finding was that the headboard fairing must maintain the low-pressure suction region around the upstream side vents as this is fundamental to the level of air extraction seen, especially in hot and humid conditions.

#### **4.6 Challenges and Future Work**

The results presented in this paper demonstrate the valuable role of Computational Fluid Dynamics in determining passive ventilation within small livestock trailers. This technology offered insight into the differences in ventilation throughout the trailer which are of potential use to trailer manufacturers and policy makers. However, it is important to appreciate that the above analyses are isothermal in nature and so the effects of internal heat and moisture build-up are neglected. Thermal considerations are critical for stationary vehicles where buoyancy-driven thermal plumes are responsible for the rate of air exchange across vent apertures (Randall and Patel, 1994). For the range of vehicle speeds already considered, it is unlikely that these buoyancy effects will dramatically influence the ventilation patterns, as they occur

through forced convection which is the dominant mechanism. Nevertheless, ventilation patterns alone are not necessarily good indicators of animal welfare. Even at high vehicle speeds, factors such as heat production, moisture generation and the build-up of pollutants including ammonia and CO<sub>2</sub> are much more closely related to heat and cold stress (Kettlewell and Mitchell, 2008). Therefore it is important to characterise the thermal micro-environment within livestock trailers so that the biological requirements of the animals themselves are considered. These aspects are the subject of continued research.

## **5. Conclusion**

Characterising natural ventilation within passively-ventilated livestock trailers is important for identifying potential issues to animal welfare. Following a series of numerical simulations, ventilation was analysed using three methods, all of which highlighted a marked difference in ventilation patterns between the upper and lower decks. Overall ventilation is better on the upper deck and numerical results suggest that current livestock transport regulations are satisfied at moderate to high vehicle speeds. In contrast, ventilation is significantly reduced on the lower deck and potentially below the regulatory threshold, particularly at lower transport speeds. The improved ventilation on the upper deck is aided by a rear tailboard vent which is effective at extracting internal airflow from the trailer. The lack of such a vent on the lower deck, coupled with small pressure gradients along the trailer sides, are responsible for the reduced ventilation seen. These results are of potential interest to livestock trailer manufacturers and policy makers which may inform future design trends.

## **Acknowledgements**

The authors would like to thank Dr J. L. Summers, Dr G. J. Blyth and Mr T. Allwood for their time and commitment in ensuring the smooth running of computer hardware during the course of this work. The study would not have been possible without the financial support of the Department for the Environment, Food and Rural Affairs (DEFRA) under grant reference number AW0933.

## **References**

AIAA, 2002, Guide for the Verification and Validation of Computational Fluid Dynamics Simulations, *American Institute of Aeronautics and Astronautics*, Guide G-077-1998(2002).

Anon. 2006. The Welfare of Animals (Transport) (England) Order 2006, Statutory Instrument No. 3260. Her Majesty's Stationery Office, London, 12 pp.

ANSYS. 2015.

<http://www.ansys.com/Products/Simulation+Technology/Fluid+Dynamics/Fluid+Dynamics+Products/ANSYS+Fluent>. Accessed 11.08.2015.

ANSYS Fluent. 2013. ANSYS Fluent Theory Guide. ANSYS Inc, Canonsburg, PA.

ASME, 2009. Standard for verification and validation in computational fluid dynamics and heat transfer. The American Society of Mechanical Engineers, ASME V&V 20-2009.

Baker C. J, Dalley S, Yang X, Kettlewell P. J and Hoxey R, 1996, An Investigation of the Aerodynamic and Ventilation Characteristics of Poultry Transport Vehicles: Part 2, Wind Tunnel Experiments, *Journal of Agricultural Engineering Research*, 65, pp. 97-113.

Dalley S, Baker C. J, Yang X, Kettlewell P. J and Hoxey R, 1996, An Investigation of the Aerodynamic and Ventilation Characteristics of Poultry Transport Vehicles: Part 3, Internal Flow Field Calculations, *Journal of Agricultural Engineering Research*, 65, pp. 97-113.

DEFRA. 2012. Keeping Farmed Animals – Guidance, Live Transport: Welfare Regulations, *Department for Environment Food & Rural Affairs*. [www.gov.uk/farm-animal-welfare-during-transportation](http://www.gov.uk/farm-animal-welfare-during-transportation) accessed 11/08/2015.

European Union 2005. Council Regulation (EC) No. 1/2005 of 22 December 2004 on the protection of animals during transport and related operations and amending Directives 64/432/EEC and 93/119/EC and Regulation (EC) No. 1255/97. Off J, L3, 05/01/2005, 1-44.

ERCOFTAC. 2000. Special Interest Group on “Quality and Trust in Industrial CFD” Best Practice Guidelines. European Research Community on Flow, Turbulence and Combustion. Eds. Casey, M., Wintergerste, T.

Gilkeson C. A, Wilson M. C. T, Thompson H. M, Gaskell P. H, Barnard R. H, Hackett K. C and Stewart D. H, 2006, Ventilation of Small Livestock Trailers, *Proceedings of the 6th MIRA International Vehicle Aerodynamics Conference*, Gaydon, UK, pp. 138-147, ISBN 0-952-41563-1.

Gilkeson C. A, Thompson H. M, Wilson M. C. T, Gaskell P. H and Barnard R. H, 2009, An

Experimental and Computational Study of the Aerodynamic and Passive Ventilation Characteristics of Small Livestock Trailers, *Journal of Wind Engineering and Industrial Aerodynamics*, 97, pp. 415-425.

Gilkeson C.A. 2009. Analysis and Optimization of Ventilation and Drag in Small Livestock Trailers Using Computational Fluid Dynamics. Ph.D. thesis. University of Leeds, United Kingdom.

Gilkeson C. A, Toropov V.V., Thompson H. M, Wilson M. C. T, Foxley N. A. and Gaskell P. H., 2013, Multi-objective Aerodynamic Shape Optimization of Small Livestock Trailers, *Engineering Optimization*, 45, pp. 1309-1330.

Hoxey R. P, Kettlewell P. J, Meehan A. M, Baker C. J and Yang X, 1996, An Investigation of the Aerodynamic and Ventilation Characteristics of Poultry Transport Vehicles: Part 1, Fullscale Measurements, *Journal of Agricultural Engineering Research*, 65, pp. 77-83.

Kettlewell P. J, Hoxey R. P and Mitchell M. A, 2000, Heat Produced by Broiler Chickens in a Commercial Transport Vehicle, *Journal of Agricultural Engineering Research*, 75, pp. 315-326.

Kettlewell P. J, Hoxey R. P, Hampson C. J, Green N. R, Veale B. M and Mitchell M. A, 2001, Design and Operation of a Prototype Mechanical Ventilation System for Livestock Transport Vehicles, *Journal of Agricultural Engineering Research*, 79, pp. 429-439.

Leonard B. P, 1979, A Stable and Accurate Convective Modelling Procedure Based on Quadratic Upstream Interpolation, *Computer Methods in Applied Mechanics and Engineering*, 19, pp. 59-98.

Mitchell M. A and Kettlewell P. J. 2008, Engineering and Design of Vehicles for Long Distance Road Transport of Livestock (Ruminants, Pigs and Poultry). *Veterinaria Italiana*, 44(1), pp. 201-213.

Norton T., Kettlewell, P., Mitchell. M. 2013. A Computational Analysis of a Fully-Stocked Dual-Mode Ventilated Livestock Vehicle During Ferry Transportation. *Computers and Electronics in Agriculture*. 93, pp 217-228.

Patankar S. V and Spalding D. B, 1972, A Calculation Procedure for Heat, Mass and Momentum Transfer in Three-Dimensional Parabolic Flows, *International Journal of Heat and Mass Transfer*, 15(10), pp. 1787-1806.

Purswell J. L, Gates R. S, Lawrence L. M, Stombaugh T. S, Coleman R. J and Adam, W. C,

2005, Air Exchange Rate in a Horse Trailer During Transport, *Proceedings of the 7th International Symposium: Livestock Environment VII*, Beijing 18-20th May, pp. 13-20.

Quinn A. D and Baker C. J, 1997, An Investigation of the Ventilation of a Day-Old Chick Transport Vehicle, *Journal of Wind Engineering and Industrial Aerodynamics*, 67&68, pp. 305-311.

Randall J. M and Patel R, 1994, Thermally Induced Ventilation of Livestock Transporters, *Journal of Agricultural Engineering Research*, 57, pp. 99-107.

Roache P.J, 1994, Perspective: a method for uniform reporting of grid refinement studies. *Journal of Fluid Engineering*, 116, pp. 405–13

Short C. A., Noakes C. J., Gilkeson C. A., and Fair A. 2014. Functional Recovery of a Resilient Hospital Type. *Building Research & Information*, 42, pp 657-684.

Spalart P. R and Allmaras S. A, 1992, One-Equation Turbulence Model for Aerodynamic Flows, AIAA Paper No. 92-0439.

Warriss P. D, Brown S. N., Knowles T. G., Wilkins L. J., Pope S. J., Chadd S. A., Kettlewell P. J., Green N. R. Comparison of the Effects of Fan-Assisted and Natural Ventilation on the Welfare of Pigs Being Transported to Slaughter. *Veterinary Record*, 158, pp 585-588.

Wheeler E. F, 2003, Horse Stable Ventilation, State College Pa: The Pennsylvania State University Agricultural and Biological Engineering Extension. Publication UB039.